June 1997 • NREL/SR-520-23172

Thin-Film Amorphous Silicon Alloy Research Partnership

Phase II
Annual Technical Progress Report
2 February 1996 - 1 February 1997

S. Guha
United Solar Systems Corporation
Troy, Michigan

National Renewable Energy Laboratory
1617 Cole Boulevard
Golden, Colorado 80401-3393
A national laboratory of
the U.S. Department of Energy
Managed by Midwest Research Institute
for the U.S. Department of Energy
under Contract No. DE-AC36-83CH10093

NREL/SR-520-23172 • UC Category: 1263 • DE97006933

Thin-Film Amorphous Silicon Alloy Research Partnership

Phase II
Annual Technical Progress Report
2 February 1996 - 1 February 1997

S. Guha
United Solar Systems Corporation
Troy, Michigan

NREL technical monitor: K. Zweibel

National Renewable Energy Laboratory
1617 Cole Boulevard
Golden, Colorado 80401-3393
A national laboratory of
the U.S. Department of Energy
Managed by Midwest Research Institute
for the U.S. Department of Energy
under Contract No. DE-AC36-83CH10093

Prepared under Subcontract No. ZAF-5-14142-01
June 1997

This publication was reproduced from the best available camera-ready copy submitted by the subcontractor and received no editorial review at NREL.

NOTICE

This report was prepared as an account of work sponsored by an agency of the United States government. Neither the United States government nor any agency thereof, nor any of their employees, makes any warranty, express or implied, or assumes any legal liability or responsibility for the accuracy, completeness, or usefulness of any information, apparatus, product, or process disclosed, or represents that its use would not infringe privately owned rights. Reference herein to any specific commercial product, process, or service by trade name, trademark, manufacturer, or otherwise does not necessariiy constitute or imply its endorsement, recommendation, or favoring by the United States government or any agency thereof. The views and opinions of authors expressed herein do not necessarily state or reflect those of the United States government or any agency thereof.

Available to DOE and DOE contractors from:
Office of Scientific and Technical Information (OSTI)
P.O. Box 62
Oak Ridge, TN 37831
Prices available by calling (423) 576-8401

Available to the public from:
National Technical Information Service (NTIS)
U.S. Department of Commerce
5285 Port Royal Road
Springfield, VA 22161
(703) 487-4650

Printed on paper containing at least 50% wastepaper, including 20% postconsumer waste

Preface

This Annual Subcontract Report covers the work performed by United Solar Systems Corp. for the period 2 February 1996 to 1 February 1997 under DOE/NREL Subcontract No. ZAF-5-14142-01. The following personnel participated in the research program.

> E. Akkashian, A. Banerjee, E. Chen, T. Glatfelter, S. Guha (Principal Investigator), M. Haag, G. Hammond, N. Jackett, H. Laarman, M. Lycette, J. Noch, D. Wolf, J. Yang, and K. Younan.

We would like to thank V. Trudeau for preparation of this report.

Table of Contents

List of Figures

List of Tables

Executive Summary

Objectives

The principal objective of this R&D program is to expand, enhance and accelerate knowledge and capabilities for the development of high-performance, two-terminal multijunction amorphous silicon (a-Si) alloy modules. The near-term goal of the program is to achieve 12% stable module efficiency by 1998 using the multijunction approach.

Approach

The major effort of the program is to develop high efficiency component and triple-junction cells with uniform property over large area so as to facilitate fabrication of monolithic modules of one-square-foot area. The component cells use materials of different bandgaps and incorporate Ge for the middle and the bottom cells. In order to reduce manufacturing cost by lowering material cost, improving throughput and minimizing optical and electrical losses associated with module fabrication, a novel laser-drilling approach has been developed and is being optimized. Investigations of long-term reliability of the modules through accelerated testing form an integral part of the program.

Status/Accomplishments

- Arrays of high efficiency component cells have been made over one-square-foot areas. Single-junction top cells have been made with an average stabilized power density of 51 W/m^2 measured under global AM1.5 illumination. Single-junction middle cells have been optimized to give average stabilized power density of 34 W/m^2 under global AM1.5 illumination with a cut-on filter with $\lambda > 530$ nm. Both these arrays are made on stainless steel substrate without any back reflector. Single-junction bottom cells have been fabricated on Ag/ZnO back reflectors with an average power density of 36 W/m^2 as measured under global AM1.5 illumination with a cut-on filter with $\lambda > 630$ nm.

- Arrays of high efficiency triple-junction cells of 0.25 cm^2 active-area have been fabricated over one-square-foot area with average stabilized efficiency of 11.6% as measured under AM1.5 illumination.

- A triple-junction module of aperture area 416 cm^2 has been fabricated with an initial efficiency of 11.7%. Based on our cell degradation studies, we expect the stabilized efficiency to exceed 10.5%.

- The novel laser-drilling approach has been used successfully to fabricate modules of one-square-foot area with shadow loss less than 1%.

- Reliability studies based on NREL's Interim Qualification Testing have been carried out to confirm the suitability of the module encapsulation materials and processes.

Section 1

Introduction

This report describes the research performed during Phase II of a three-phase, three-year program under NREL Subcontract No. ZAF-5-14142-01. The research program is intended to expand, enhance and accelerate knowledge and capabilities for the development of high-performance, two-terminal multijunction amorphous silicon (a-Si) alloy modules.

It is now well recognized that a multijunction, multibandgap approach has the potential of achieving the highest stable efficiency in a-Si alloy solar cells. In this approach, the bandgap of the materials of the component cells is varied in order to capture a wide spectrum of the solar photons. Significant progress has been made in the development of materials and cell design in the last few years, and a stable module efficiency of 10.2% has been demonstrated over one-square-foot area using a triple-junction approach in which the bottom two component cells use amorphous silicon-germanium (a-SiGe) alloy. In order to meet the Department of Energy goal of achievement of 12% stable module efficiency by 1998, it is necessary to make further improvements in each of the component cells.

New back reflectors also need to be developed to facilitate improved light-trapping performance. Since the aim of the program is to develop a manufacturing technology, the research work must address issues involving scaleup, reliability and cost. It should be pointed out that reliability and cost issues encompass module interconnect and encapsulation methods as well.

The research report describes the activities carried out in Phase II on various tasks that were taken up to address the above issues. In Section 2, we discuss investigations on back reflectors to improve cell performance, and investigate uniformity in performance over a one-square-foot area. In Section 3, we present results on performance of component cells, both in the initial and in the light-degraded states, deposited over a one-square-foot area. The uniformity in deposition is investigated by studying the performance of subcells deposited over the entire area. In Section 4, we present results on the performance of triple-junction cells and modules. The modules use grid-lines and encapsulants compatible with our production technology. In Section 5, we discuss the novel laser-processing technique that has been developed at United Solar to improve energy-conversion efficiency and reduce manufacturing cost. Detailed description of optimization of the processing steps is discussed, and performance of a laser-processed, triple-junction device of 12.6 cm^2 area is presented. Experimental results on investigations of reliability of modules are presented in Section 6. Future directions of the research work are outlined in Section 7.

Section 2

Back Reflector Study

Introduction

One of the essential requirements in achieving high efficiency solar cells is that the back reflector must possess high reflectivity with light trapping quality. Our present textured Ag/ZnO back reflector has these properties and does give rise to significant enhancement in the red response. In our ongoing program, we have strived to further improve the Ag/ZnO back reflector property.

In this section, we present results of our study on specularity and uniformity of one-square foot, large-area Ag/ZnO back reflector. We shall also present the red response of the state-of-the-art a-SiGe alloy solar cells on Ag/ZnO.

Specularity and Uniformity Study of Large-area Ag/ZnO Back Reflector

We have made an Ag/ZnO back reflector using the "RADLAS" machine. The deposition process consists of sequential deposition of Ag and ZnO films on a flexible large-area stainless steel substrate using a mangetron sputtering process. For uniformity studies on the back reflector, 2″ x 2″ sections are cut off and the integrated total reflectance measured as a function of wavelength. The specularity is measured in the red region using a wavelength characteristic of a He-Ne laser. Results on two different Ag/ZnO back reflectors are summarized below.

In the first example, Fig. 1 shows the reflectance in the wavelength range 800-950 nm at five different locations of a 900 cm^2 area Ag/ZnO back reflector. The values of reflectance at all the locations are in the range of 87-95 %. These values are higher than those mentioned in the August 1995 monthly report. However, the enhancement in reflectance has a trade-off. The specularity at some of the locations, as summarized in Table 1, is somewhat higher.

Table 1. Specularity Measurement at Various Locations on a 900 cm^2 Ag/ZnO Back Reflector.

Location	Specularity
NE corner	10.4%
NW	11.3%
SW	11.5%
SE	10.5%
Center	13.5%

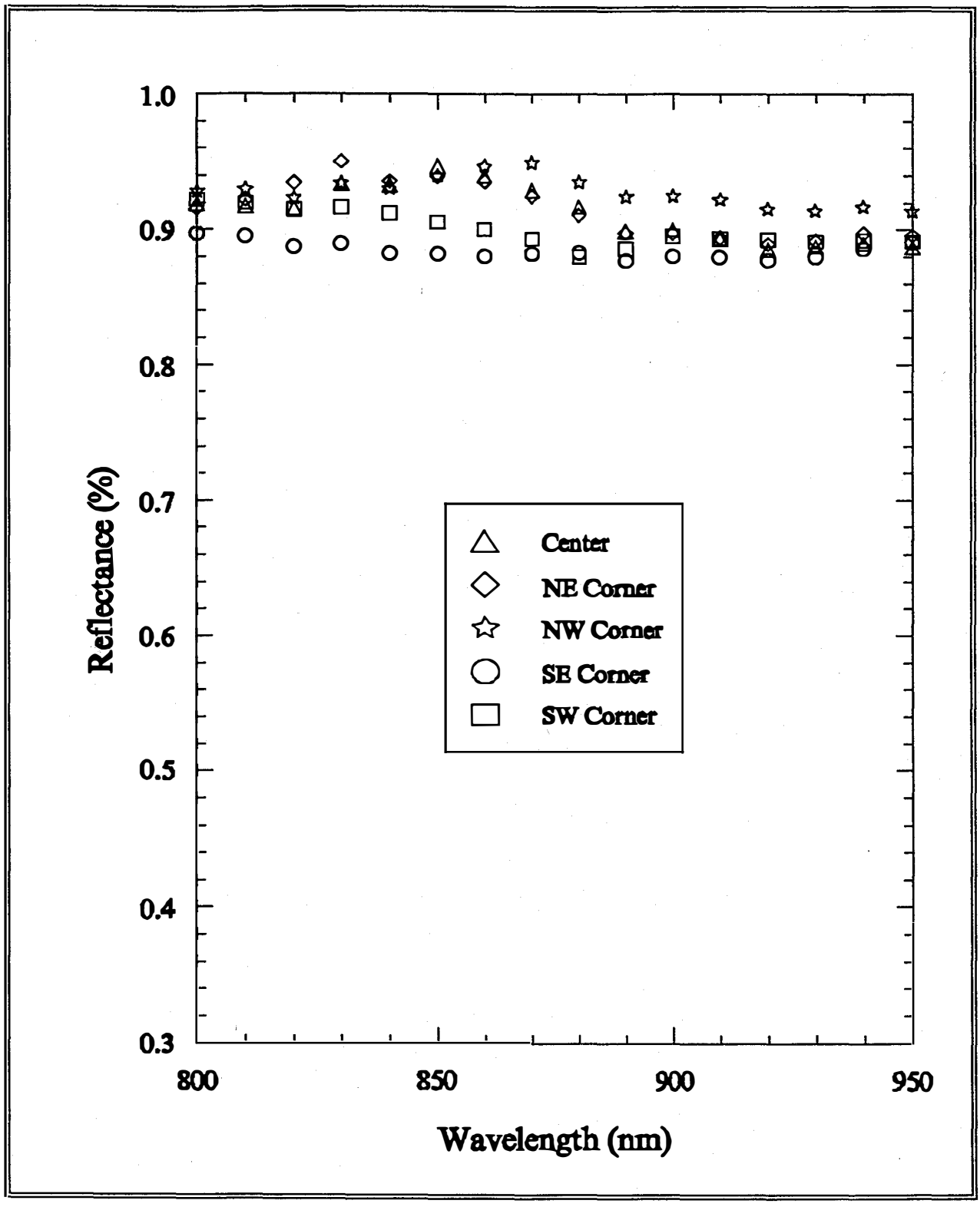

Figure 1. **Reflectance versus wavelength at several locations of a 900 cm^2 area Ag/ZnO back reflector.**

In the second example of Ag/ZnO back reflector, the representative reflectance curve of a 2"x2" piece taken from the center of a one-square-foot back reflector is shown in Fig. 2. The total integrated reflectance in the wavelength range 800-950 nm is in the range of 78-87%. The specular component is 6%. As regards uniformity issues over the one-square-foot area, we have shown in the past (Phase I Annual Report and Table 1 above) that the value of reflectance is pretty uniform over the entire one-square-foot area. The major variation in the spatial characteristics is that the center piece usually has higher specularity. Thus, it is reasonable to expect that the back reflector properties being reported here for the center piece satisfy the twin requirements of high reflectance and low specular component over the entire area.

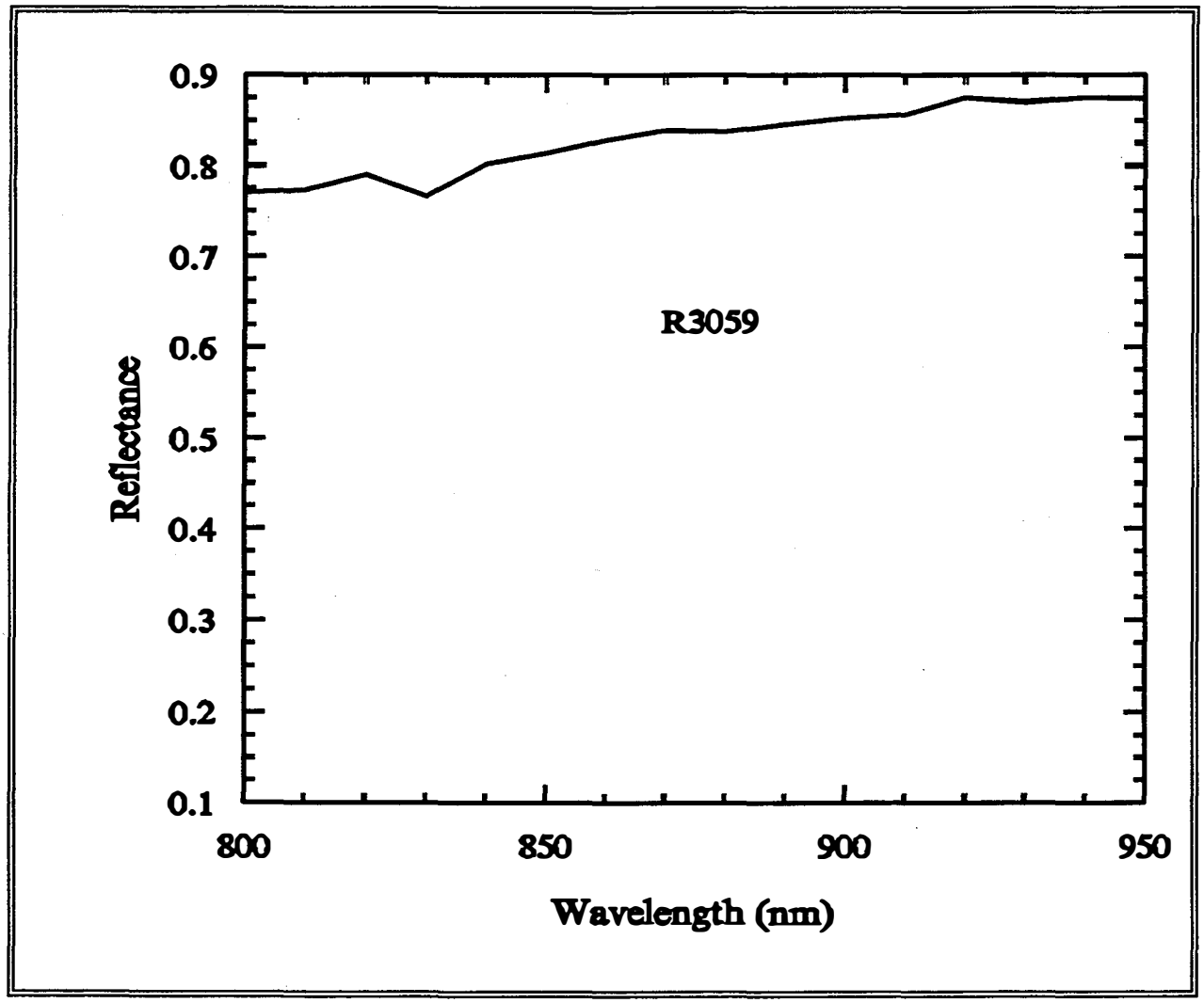

Figure 2. Reflectance versus wavelength of Ag/ZnO back reflector.

Table 2 summarizes the results of the second case and the corresponding Phase II milestone for the back reflector. It shows that the values obtained exceed the milestone requirements of "the total integrated reflectance in the 800-950 nm range is greater than 80% with specular component less than 10%."

Table 2. Summary of Ag/ZnO Back Reflector Characteristics and Phase II Milestones.

Back Reflector	Reflectance (800-950 nm) %	Specular Component (%)
R3059 Center	78-87	6
Phase II Milestone	> 80	< 10

Narrow Bandgap a-SiGe Alloy Solar Cells on Ag/ZnO with High Red Response

One of the methods to evaluate back reflectors is to deposit a narrow bandgap a-SiGe alloy solar cell and measure its quantum efficiency and evaluate its long-wavelength response. The best cell obtained to date measured under AM1.5 global illumination with a λ>630 nm cut-on filter has the following characteristics: J_{sc} = 13.1 mA/cm^2, V_{oc} = 0.622 V, FF = 0.635, and P_{max} = 5.2 mW/cm^2. This represents the highest initial power achieved for an a-SiGe alloy cell. The quantum efficiency data versus wavelength data is shown in Fig. 3. The photocurrent evaluated from this Q curve is 25.8 mA/cm^2. At λ = 850 nm, the quantum efficiency is 52%, reflecting the high quality of the back reflector. The values of J_{sc} = 13.1 mA/cm^2 for λ>630 and Q = 52% at 850 nm represent significant improvement from those reported in Phase I.

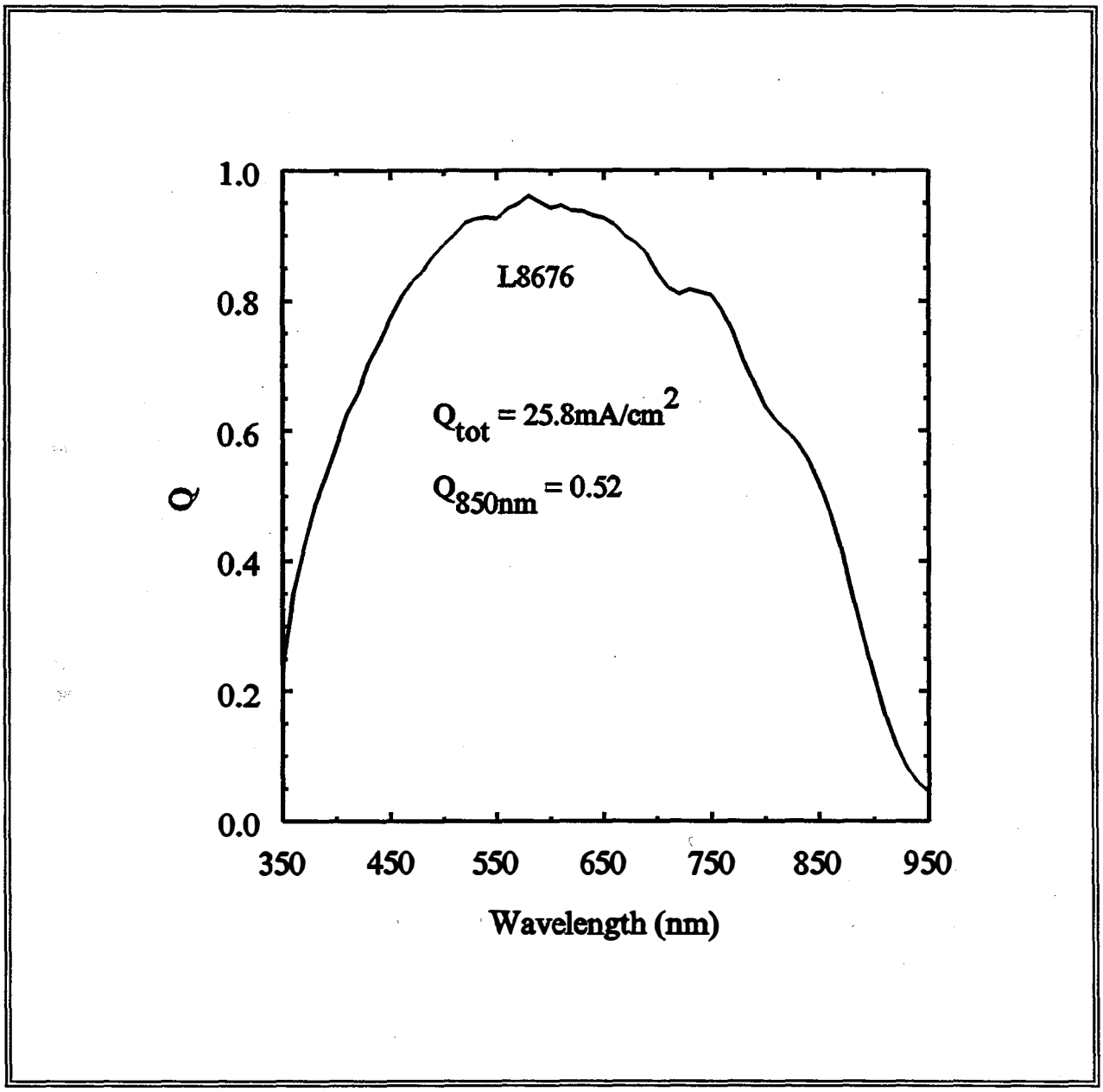

Figure 3. Quantum efficiency versus wavelength for an a-SiGe alloy cell on Ag/ZnO back reflector.

Section 3

Status of a-Si Alloy and a-SiGe Alloy Component Cells

Introduction

In order to obtain high efficiency multijunction devices for module fabrication, two conditions have to be satisfied. First, it is necessary to optimize the component top, middle, and bottom cells on appropriate substrates. Second, the uniformity of the component cell efficiency over the module area should be good. We have worked extensively on the uniformity issues during the Phase I period when the 2B machine was initially being optimized after its renovation. The results after the optimization process have been described in the Phase I Annual Report. Since the uniformity obtained is adequate, the only work done regarding uniformity issues during Phase II was the routine check from time to time that the desired uniformity was being maintained. In the following section, the new results of the component cells are described.

Device Fabrication and Measurement

The top cell results reported here have been made in the small-area LINE machine as well as the large-area 2B machine. The middle, bottom, and triple-junction cells have been made in the 2B machine. The fabrication and evaluation process of cells made in the 2B machine is summarized. The starting substrate material is a thin stainless steel (ss) sheet of approximately one-square-foot area. The back reflector (BR) consists of textured Ag/ZnO films deposited over the one-square-foot area by sputtering. The semiconductor devices are made by conventional glow discharge deposition over the entire area. The substrate is cut into 2" x 2" pieces and transparent conducting oxide (TCO) is deposited through an evaporation mask to yield devices of active area 0.25 cm^2 area. The LINE machine deposits the devices directly on the 2″ x 2″ substrates and the TCO is done the same way.

The top a-Si alloy cell is normally deposited on ss substrates with no back reflector and measured under AM1.5 condition. The rationale is that the top cell in the triple-junction configuration sees the full spectrum of the incident light but does not receive any reflected light since the underlying a-SiGe alloy cells starve it of any reflected light.

For similar reasons as for the top cell, the middle component a-SiGe alloy cell consisting of intermediate bandgap a-SiGe alloy *i* layer is also deposited on ss substrate with no back reflector. In this case, the uncertainty in the simulation is slightly higher since the middle cell in the triple-junction configuration receives a small amount of reflected light. The I-V measurements on the middle cell are made using a bandpass filter of $\lambda > 530$ nm in order to simulate the filtering effect of the incident light of the top cell.

The bottom component cell using narrow bandgap a-SiGe alloy *i* layer is deposited on a textured Ag/ZnO back reflector. The I-V measurements are made through a bandpass filter of $\lambda > 630$ nm in order to simulate the light which the device receives in the triple-junction structure.

Light Soaking

The component cells have been light-soaked to determine the stabilized values. The devices were degraded under one-sun, open-circuit, and 50 °C conditions for over 600 hours. The middle and bottom component cells were illuminated through appropriate high wavelength cut-on filters to simulate the short-circuit current density which the respective devices produce in the triple-junction configuration. The stabilized values of the top and middle cells on ss substrate and the bottom cell on BR are reported.

Initial Results of a-Si Alloy Top Cell on ss

The top cell studies can be subdivided into two categories. In the first, we have explored the effect of deposition rate on cell performance. In the second, we have further optimized the deposition parameters of the low-rate material in order to achieve higher efficiency. The devices have been made in the small-area machines and the results are described below.

Effect of Deposition Rate on Top Cell Performance

In our June, 1996 monthly report, we summarized the effect of deposition rate on top cell performance. We observed that as the deposition rate was increased from 2 Å/s to 3 Å/s, there was a decrease in V_{oc} and FF. We have further studied the 3 Å/s deposition parameters and improved on the cell characteristics. Table 3 lists the initial J-V characteristics of a-Si:H top cells with *i* layer deposited at 1, 2, 3 Å/s with the improved characteristics demonstrated in Sample #5779. The J-V characteristic for #5779 is shown in Fig. 4.

Table 3. Initial J-V Characteristics of a-SI:H Top Cells on ss with Different Deposition Rates.

Sample	Deposition Rate (Å/s)	J_{sc} (mA/cm^2)	V_{oc} (V)	FF
Baseline	~1	8.65	1.014	0.780
5635	~2	7.33	0.971	0.744
5691	~3	7.42	0.944	0.742
5779	~3	8.36	0.954	0.750

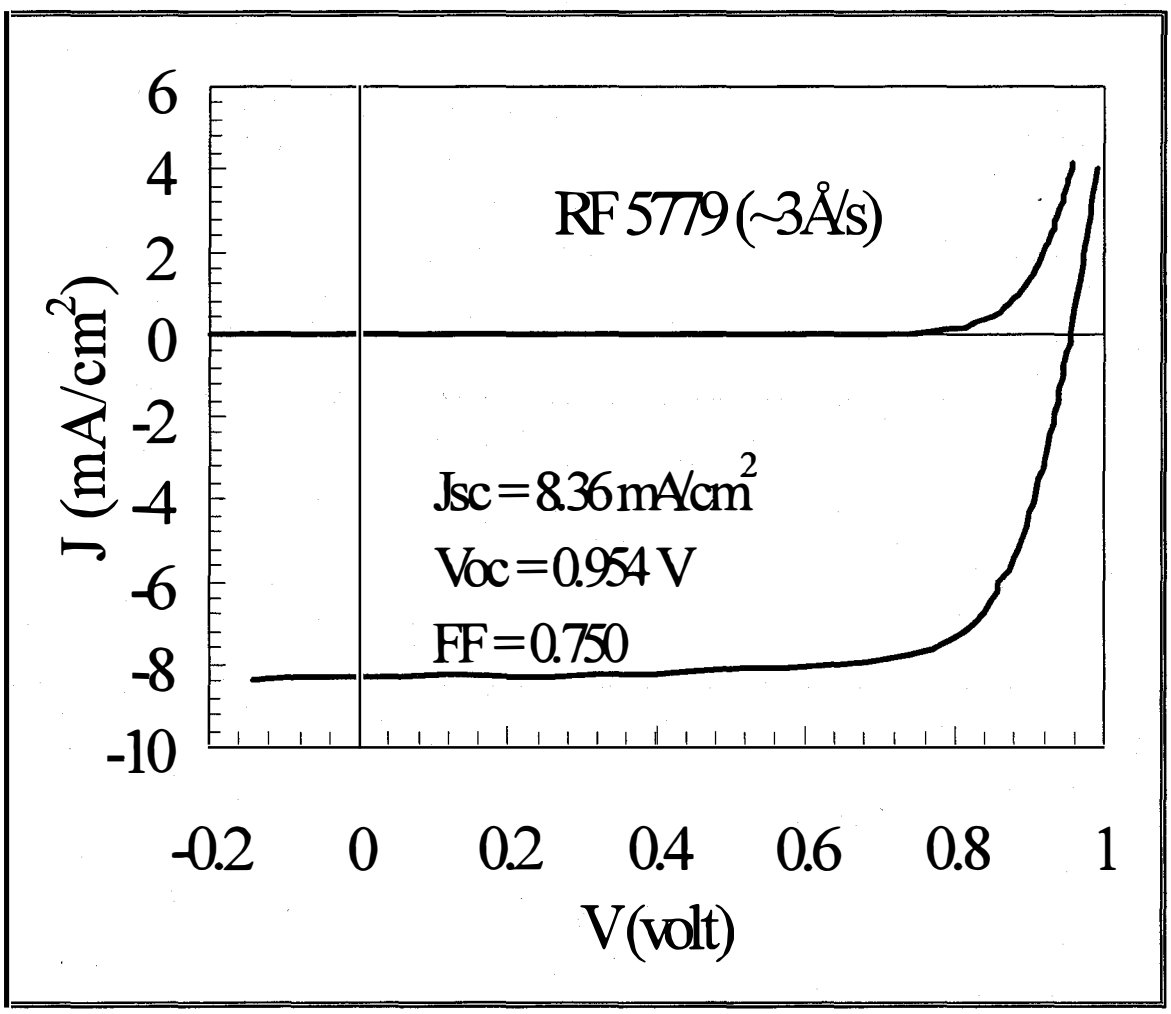

Figure 4. J-V characteristics of an a-Si:H cell with deposition rate of 3Å/s.

Low Deposition Rate Top Cell

From our earlier studies in the design of a triple-junction structure, it is concluded that using the top cell as the current-limiting component cell is very desirable. The performance of the top cell, therefore, is very important. Optimization of cell parameters has led to further gains in device efficiency. The results of two improved devices are summarized in Table 4. The values of V_{oc} FF, J_{sc}, and P_{max} of device LINE 8675 are 1.011 V, 0.782, 86.8 A/m^2, and 68.6 W/m^2, respectively. These represent the highest values reported for an a-Si alloy cell of this structure. The J-V characteristics are shown in Fig. 5. The values of V_{oc}, FF, J_{sc}, and P_{max} for LINE 8777 are 0.983 V, 0.787, 84.6 A/m^2, and 65.4 W/m^2, respectively. The result of a top cell on stainless steel substrate made in the 2B machine is also shown in Table 4. The values of V_{oc}, FF, J_{sc}, and P_{max} of 2B 4568 are 1.014 V, 0.755, 80.9 A/m^2, and 61.9 W/m^2, respectively. These results represent a significant improvement over those obtained in Phase I.

Table 4. Initial Results of Top, Middle, and Bottom Component Cells of Area 0.25 cm^2.

Type	Sample #	Substrate	Measurement Spectrum	V_{oc} (V)	J_{sc} (A/m^2)	FF	P_{max} (W/m^2)
Top	L8675	ss	AM1.5	1.011	86.8	0.782	68.6
	L8777	ss	AM1.5	0.983	84.6	0.787	65.4
	2B4568	ss	AM1.5	1.014	80.9	0.755	61.9
Middle	2B4569	ss	λ>530nm	0.702	94.0	0.689	45.5
	2B4298	Ag/ZnO	λ>630nm	0.745	78.8	0.701	41.1
Bottom	2B4289	Ag/ZnO	λ>630nm	0.630	115.0	0.633	45.9

a-SiGe Alloy Middle Cell on ss

The initial results of the a-SiGe alloy middle cell on both ss and Ag/ZnO BR are summarized in Table 4. The device performance under AM1.5 illumination using $\lambda > 530$ nm (for stainless steel) and $\lambda > 630$ nm (for Ag/ZnO back reflector) cut-on filters are shown. The values of V_{oc}, J_{sc}, FF, and P_{max} for the ss case with $\lambda > 530$ nm are 0.702 V, 94.0 A/m^2, 0.689, and 45.5 W/m^2, respectively. The values of V_{oc}, J_{sc}, FF, and P_{max} for the BR case with $\lambda > 630$ nm are 0.745 V, 78.8 A/m^2, 0.701, and 41.1 W/m^2, respectively. These values demonstrate the significant improvements over the Phase I results. The superior results are attributed to improvement in the material quality of the a-SiGe alloy incorporating more Ge than used before. The enhanced Ge content in the intrinsic layer results in extended red response without any significant deleterious effect on the current collection.

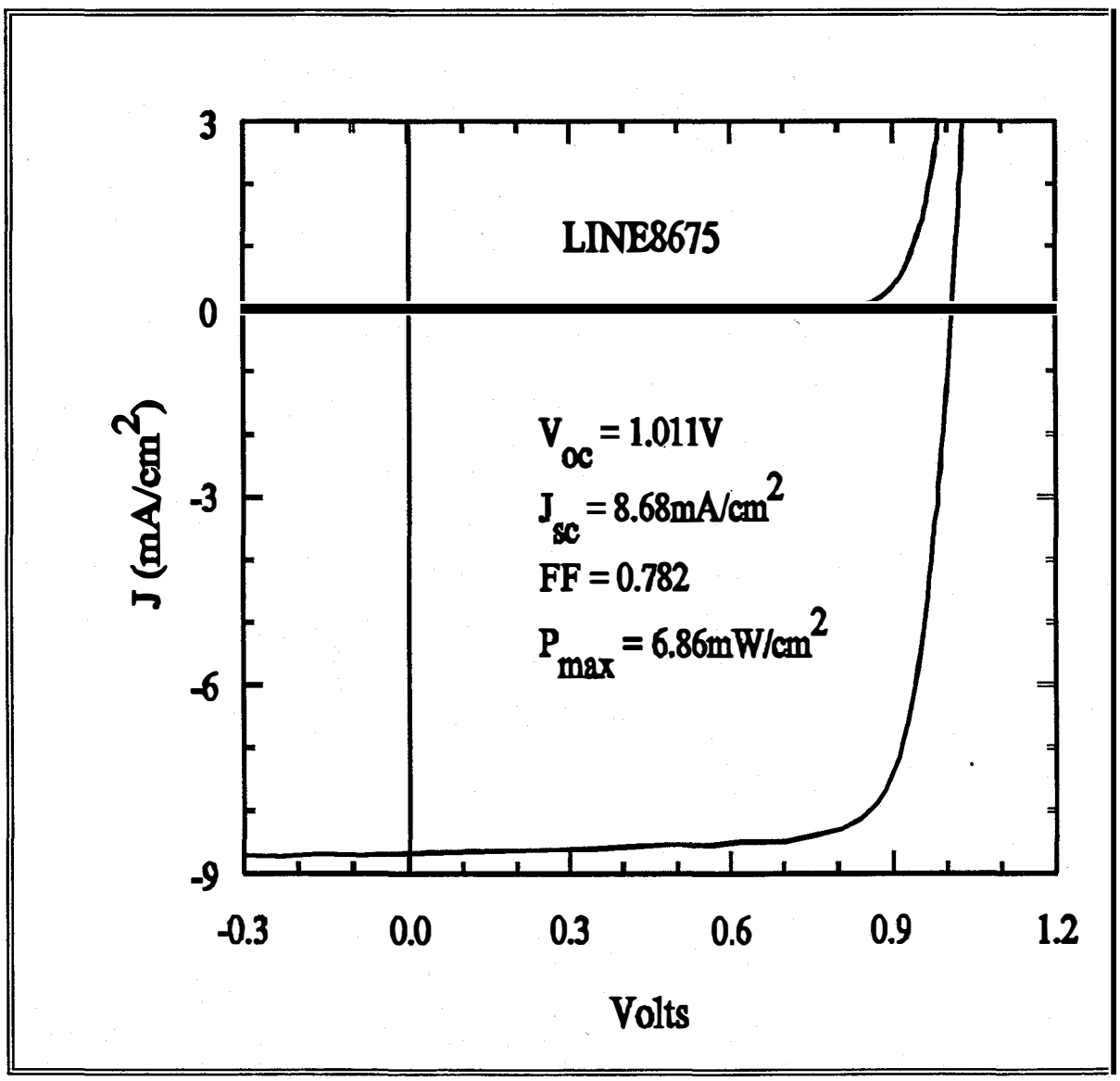

Figure 5. **Initial J-V characteristic of an a-Si alloy top cell on stainless steel.**

a-SiGe Alloy Bottom Cell on Back Reflector

The initial performance of the bottom a-SiGe alloy narrow bandgap cell on Ag/ZnO BR are summarized in Table 4. The device performance under AM1.5 illumination using $\lambda > 630$ nm is given. The values of V_{oc}, FF, J_{sc} (from Q measurements), and P_{max} are 0.630 V, 0.633, 115.0 A/m^2, and 45.9 W/m^2, respectively. These values represent significant improvement over the devices reported in Phase I. As in the case of the middle cell, the success is attributed to the achievement of high quality a-SiGe alloy of narrower bandgap than was possible in the past. The new device responds to even longer wavelength photons.

Stabilized Results of the Component Cells

The stabilized results of the top, middle, and bottom component cells are summarized in Table 5. For the purpose of comparison, the corresponding Phase II milestones are also tabulated. It may be noted that the best devices (highest initial efficiency) have not been subjected to light-soaking. The initial performance (P_{max} only) of the best devices (taken from Table 4) are also shown in the table. Comparison of the initial values of P_{max} of the best devices with those that have actually been light-soaked demonstrates that the stabilized efficiency of the best devices is expected to be higher than that being reported for all the categories.

The stabilized results of two top cells--one from the LINE machine and the other from the 2B machine--are shown in Table 5. Sample L5777 was deposited on textured substrate coated with Cr. Sample 2B 2516 was deposited directly on stainless steel. The AM1.5 results of LINE 5777 are V_{oc} = 0.97 V, FF = 0.72, J_{sc} = 73 A/m^2, and P_{max} = 51 W/m^2. The results of 2B 2516 are V_{oc} = 0.93 V, FF = 0.69, J_{sc} = 78 A/m^2, and P_{max} = 51 W/m^2. The Phase II goal is V_{oc} = 0.94 V, FF = 0.70, J_{sc} = 78 A/m^2, and P_{max} = 51 W/m^2. Thus, the top cell results meet the milestone requirement. The initial P_{max} of 62 W/m^2 for the best device 2B 2516 is markedly higher than the corresponding value of 56 W/m^2 for 2B 2516. The stabilized result of 2B 4568 is expected to be higher than that of 2B 2516.

The stabilized results of the middle cell 2B 2586 on stainless steel are summarized in Table 5. The I-V characteristics were measured under AM1.5 illumination using a 530 nm cut-on filter. The cell parameters are V_{oc} = 0.73 V, FF = 0.60, J_{sc} = 78 A/m^2, and P_{max} = 34 W/m^2. The Phase II goal is V_{oc} = 0.73 V, FF = 0.59, J_{sc} = 78 A/m^2, and P_{max} = 34 W/m^2. Thus, the middle cell results meet the requirement of the milestone. The initial P_{max} of 45 W/m^2 for the best device 2B 4569 is higher than the corresponding value of 43 W/m^2 for sample 2B 2586. It is, therefore, expected that the stabilized result of the best device will be better than that of 2B 2586.

The stabilized results of the bottom cell 2B 2484 on Ag/ZnO back reflector are summarized in Table 5. The measurements were made under AM1.5 illumination using a 630 nm cut-on filter. The device performance is V_{oc} = 0.64 V, FF = 0.57, J_{sc} = 99 A/m^2, and P_{max} = 36 W/m^2. The Phase II goal is V_{oc} = 0.65 V, FF = 0.59, J_{sc} = 82 A/m^2, and P_{max} = 31 W/m^2. Therefore, the bottom cell satisfies the milestone requirement. The best device 2B 4289 has an initial P_{max} of 46 W/m^2 which is higher than that of 2B 2484. The stabilized result of 2B 4289 is expected to be better than that of 2B 2484.

Table 5. Stabilized Results of the Top, Middle, and Bottom Component Cells.

Sample #	Area (cm^2)	Measurement Spectrum	V_{oc} (V)	FF	J_{sc} (A/m^2)	P_{max} (W/m2)	
						Stable	Initial
Top cell on ss							
L5777*	0.25	AM1.5	0.97	0.72	73	51	
2B2516	0.82	AM1.5	0.93	0.69	78	51	56
2B4568	0.25	AM1.5					62
Phase II Goal	1	AM1.5	0.94	0.70	78	51	
Middle cell on ss							
2B2586	1	λ>530nm	0.73	0.60	78	34	43
2B4569	0.25	λ>530nm					45
Phase II Goal	1	λ>530nm	0.73	0.59	78	34	
Bottom cell on BR							
2B2484	0.82	λ>630nm	0.64	0.57	99	36	43
2B4289	0.25	λ>630nm					46
Phase II Goal	1	λ>630nm	0.65	0.59	82	31	

* deposited on textured substrate coated with Cr

Section 4

Status of Triple-Junction Solar Cells and Modules

Introduction

Triple-junction triple-bandgap approach has been adopted to obtain high efficiency multijunction devices. The bottom and middle cells employ narrow bandgap and intermediate bandgap a-SiGe alloy *i* layers, respectively. The top cell uses a-Si alloy *i* layer. The status of the initial efficiency and stabilized efficiency of the component cells have been described in Section 3. In this section, the status of the triple-junction devices and modules are described. An initial module efficiency of 11.7% has been obtained.

Triple-junction Solar Cells

The triple-junction devices have been made in the 2B machine using a procedure similar to the one used for component cells as described in Section 3. Representative 2" x 2" substrates have been cut out for evaluation. All the devices have been fabricated on Ag/ZnO BR and the active area of the devices is 0.25 cm^2. For best performance, the device should be top-cell current limited. The current contributions from the top, middle, and bottom cells have been obtained from Q versus wavelength measurements. The current density of the limiting cell has been used as the short-circuit current density of the device. The stabilized values have been obtained after more than 1300 hours of one-sun illumination under 50 °C and open-circuit conditions.

Table 6 summarizes the initial and stabilized results of triple-junction devices measured under AM1.5 conditions. Two of the highest initial efficiency devices, 2B 4359 and 2B 4374, have not been light-soaked. Only the initial results are presented. The performance of sample 2B 4359 is V_{oc} = 2.329 V, J_{sc} = 79.2 A/m^2, FF = 0.721, and efficiency = 13.30%. The current density contributions, as determined from quantum efficiency measurements, from the top, middle, and bottom cells are 7.92, 8.17, and 9.10 mA/cm^2. The current density of the limiting cell, Q_{top} = 79.2 A/m^2, is used as the current density of the device. Sample 2B 4374 exhibits an efficiency of 13.52% which is the highest ever obtained in the 2B machine. The values of V_{oc}, J_{sc}, and FF are 2.291 V, 83.7 A/m^2, and 0.705, respectively. The current-density contributions of the top, middle, and bottom cells are 8.51, 8.48, and 8.37 mA/cm^2. The J-V characteristics and Q curves of 2B 4374 are shown in Fig. 6. The initial and stabilized results of sample 2B 4289 are summarized in Table 6. The Phase II goal of 11.50% stabilized efficiency is also shown. The stable efficiency of 2B 4289 is 11.58% which meets the Phase II milestone. The initial efficiency of the device was 13.26% which is slightly lower than those of 2B 4359 and 2B 4374. The degradation characteristics of 2B 4389 as a function of light-soaking time is shown in Fig. 7. The total degradation after 1337 hours of exposure is 12.7% of its initial value. Saturation occurs after approximately 400 hours.

Table 6. Initial and Stabilized Results of 0.25cm^2 Area Triple-junction Devices made on Ag/ZnO BR.

Sample #	Status	Voc (V)	Jsc (A/m2) Top/Middle/Bottom (mA/cm^2)	FF	Efficiency (%)
2B4359	Initial	2.329	79.2 7.92/8.17/9.10	0.721	13.30
2B4374	Initial	2.291	83.7 8.51/8.48/8.37	0.705	13.52
2B4289	Initial	2.33	80.2 8.02/8.24/8.93	0.71	13.26
	Stable	2.26	80.4	0.64	11.58
Phase II Goal	Stable				11.50

Triple-junction Modules

Initial Results

Extensive work has been done on developing a ~900 cm^2 aperture-area module which would pass the Interim Qualification Test Standard NREL/TR-213-3624 and also be production compatible. The primary focus of modules fabricated in the past was to obtain high stabilized efficiency, and there was no emphasis on qualification testing or production compatibility. The new design addresses both these important issues. The module design, assembly processes, structure, and materials used are similar to those being used in manufacturing. The new module design has come at a cost—the module optical losses are higher. Consequently, the module efficiency is lower even with the same or even slightly improved small-area device efficiency. Thus, any comparison of present module efficiency with that in the past must be done with some care.

The module design consists of a single one-square-foot, triple-junction monolithic device deposited on a stainless steel substrate with Ag/ZnO back reflector. There are no interconnections. The current is collected from the top using grid wires and bus bars. The device is encapsulated to form a module of aperture ≥900 cm^2 and in which a layer of EVA/Tefzel is used as the encapsulant.

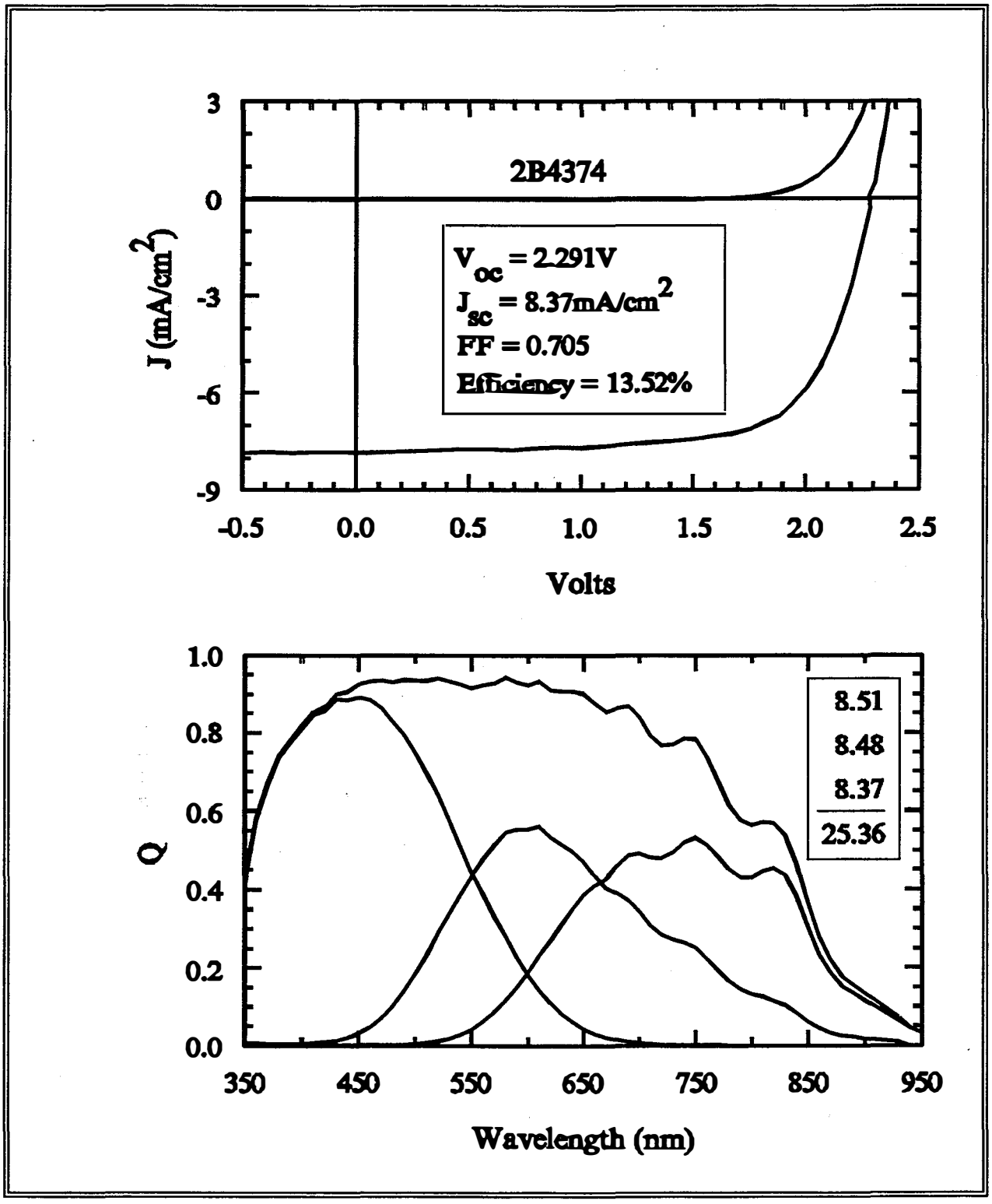

Figure 6. J-V characteristics and Q curves of triple-junction device with initial efficiency of 13.52%.

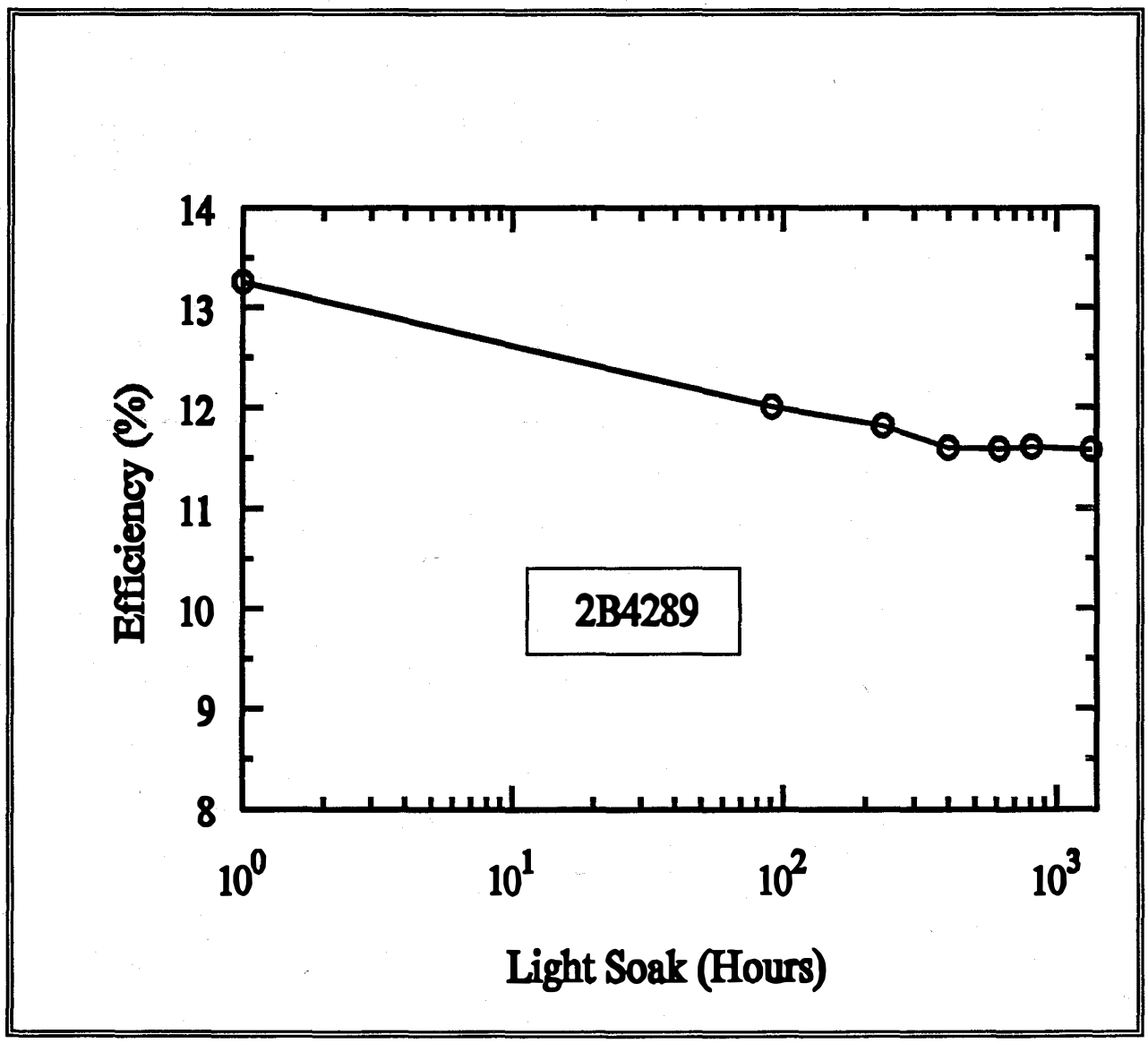

Figure 7. Stability of triple-junction devices after 1337 hours of light-soak.

Table 7 summarizes the initial results of the modules with efficiency of 9.8% and above. All the results are initial values and have been measured using a Spire solar simulator Model 240A with a peak detector circuit board.

The table shows that Module #4067 exhibits the highest aperture area efficiency of 10.5%. The corresponding values of V_{oc}, I_{sc}, and FF are 2.32 V, 6.07 A, and 0.680, respectively. The I-V characteristics of the module are shown in Fig. 8. It may be noted that two of the modules listed in Table 7 exhibited an efficiency of 11.0% at the pre-lamination stage which is the highest ever obtained in the 2B machine. After lamination, the efficiency dropped to 10.5 and 10.2%.

Table 7. Summary of Initial Triple-Junction Module Results.

Module #	Aperture Area (cm^2)	V_{oc} (V)	I_{sc} (A)	FF	Efficiency (%)
3969	972	2.31	6.40	0.646	10.2
3987	972	2.34	6.38	0.666	10.2
3994	972	2.36	6.19	0.648	9.8
3995	972	2.37	6.18	0.666	10.0
3999	976	2.32	6.30	0.654	9.8
4000	978	2.31	6.32	0.659	9.8
4014	909	2.29	6.01	0.656	9.9
4016	909	2.32	5.88	0.670	10.1
4020	909	2.31	5.94	0.672	10.2
4021	909	2.32	5.90	0.684	10.3
4039	909	2.31	6.03	0.664	10.2
4040	909	2.27	6.02	0.662	9.9
4047	909	2.30	5.86	0.664	9.9
4052	909	2.25	6.12	0.645	9.8
4056	909	2.29	6.09	0.646	9.9
4067	909	2.32	6.07	0.680	10.5
4070	909	2.29	6.04	0.670	10.2
4073	909	2.30	5.78	0.698	10.2
4473	909	2.21	6.32	0.642	9.9
4526	909	2.26	6.24	0.648	10.0

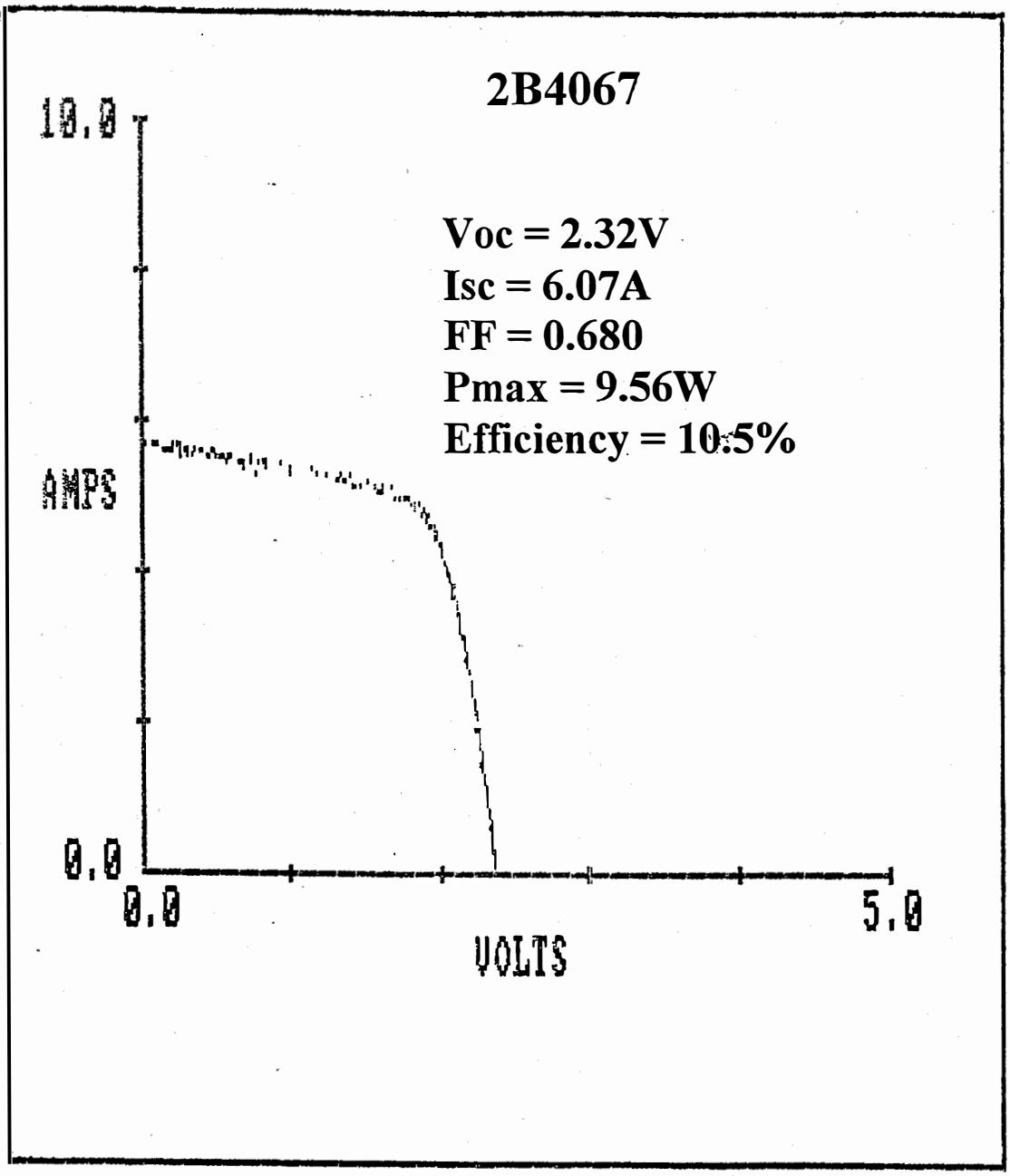

Figure 8. I-V characteristics of module 2B 4067.

Stabilized Results

A few of the modules were subjected to light-soaking under one-sun illumination, open-circuit, and 50 °C conditions. For comparison, a couple of modules were fabricated using double-junction, similar bandgap a-Si/a-Si alloy devices made in our roll-to-roll production machine. The module assembly of the 2B and production TA material was done in an identical manner. All the modules were light-soaked under identical conditions. The stabilized results after ~1000 hours of exposure of three 2B and two TA modules are summarized in Table 8. The stabilized efficiency of the 2B modules are 9.1-9.3% In comparison, the production TA modules stabilize at 5.8-5.9%. Further, the degradation of the 2B modules is only ~8.1-9.8% as compared to a corresponding value of 18.6-19.4% for the TA modules. These results demonstrate the advantage of the triple-junction, triple-bandgap approach. The stabilized results are shy of the Phase II goal. This is partly attributed to the new module design which incorporates higher losses. Efforts are under way to bridge this gap. Figure 9 shows a plot of the module P_{max} as a function of light-exposure time for all the modules. The modules exhibit substantial saturation.

Table 8. Stabilized Results of Modules after Light-Soak.

Module #	Hours	V_{oc}	I_{sc} (A)	FF	P_{max} (W)	Efficiency (%)	Degradation in P_{max} (%)
2B3987	903	2.30	6.22	0.625	8.93	9.2	9.8
2B4020	1067	2.29	5.67	0.636	8.26	9.1	8.1
2B4067	1067	2.32	5.73	0.646	8.58	9.4	8.0
TA63	1067	1.71	5.54	0.560	5.30	5.8	19.4
TA176	903	1.71	5.91	0.567	5.73	5.9	18.6
Phase II Goal						11.0	

High Efficiency Modules

The initial values of efficiency summarized in Table 7 are lower than the expected value which has been calculated on the basis of small-area device efficiency and module losses. It was concluded that the additional loss occurs due to spatial nonuniformity problems. In order to test out this hypothesis, modules of aperture area 416 cm^2 were fabricated. The initial results of three modules are summarized in Table 9. The efficiency is in the range of 11.4-11.7% and is much higher than the highest value of 10.5% obtained for module #4067 (see Fig.8). This result confirms the nonuniformity issue. The I-V characteristics of the 11.7% module is shown in Fig 10. The values of V_{oc}, I_{sc}, and FF are 2.29 V, 3.09 A, and 0.690, respectively. Light-soaking of a couple of the high efficiency modules is under way and the results will be reported later.

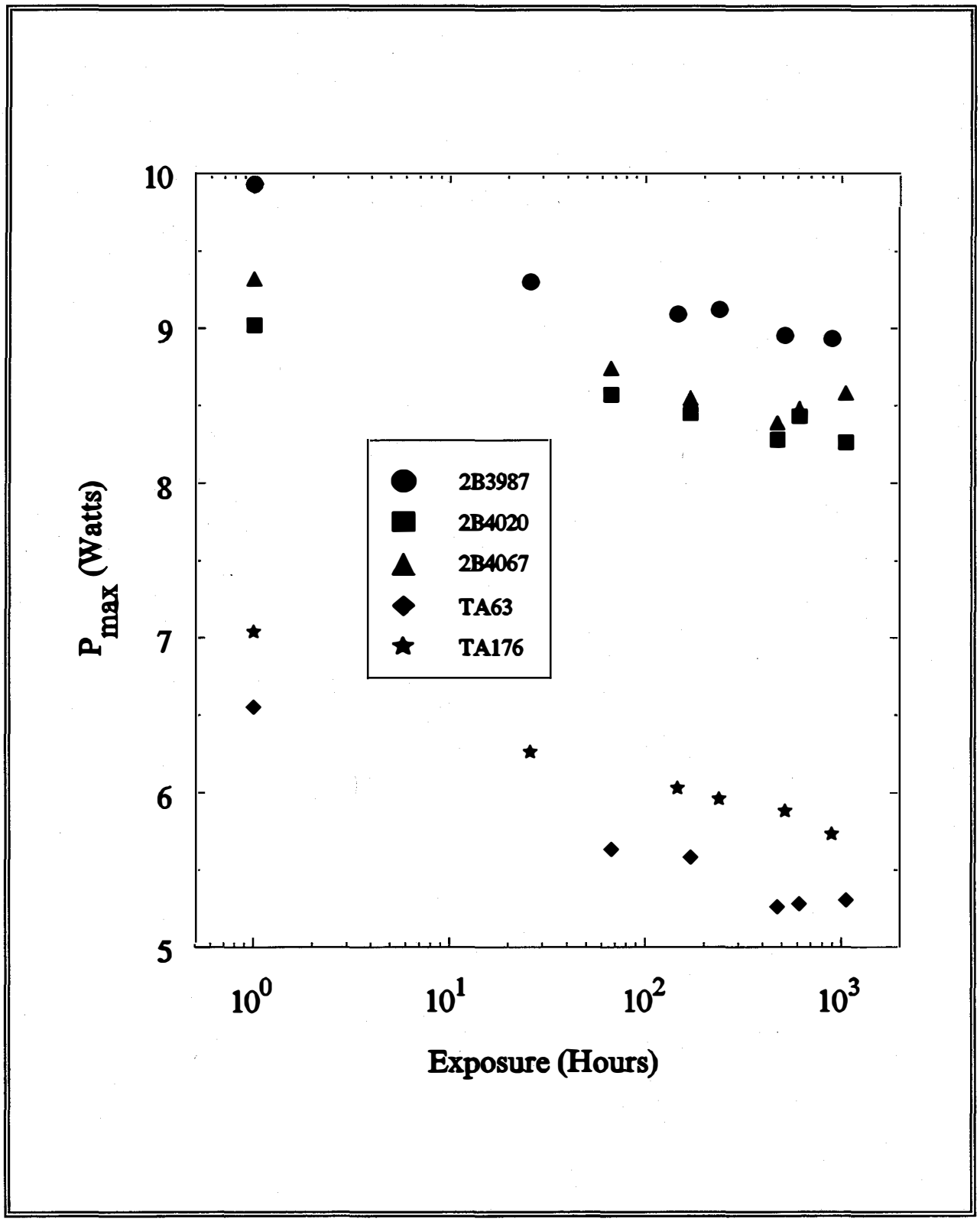

Figure 9. P_{max} as function of light-exposure time of modules.

Table. 1. Initial Results of High Efficiency Modules.

Module#	Aperture area (cm^2)	V_{oc} (V)	I_{sc} (A)	FF	Eff. (%)
4661	415	2.27	3.08	0.678	11.4
4674	416	2.30	3.07	0.684	11.6
4675	416	2.29	3.09	0.690	11.7

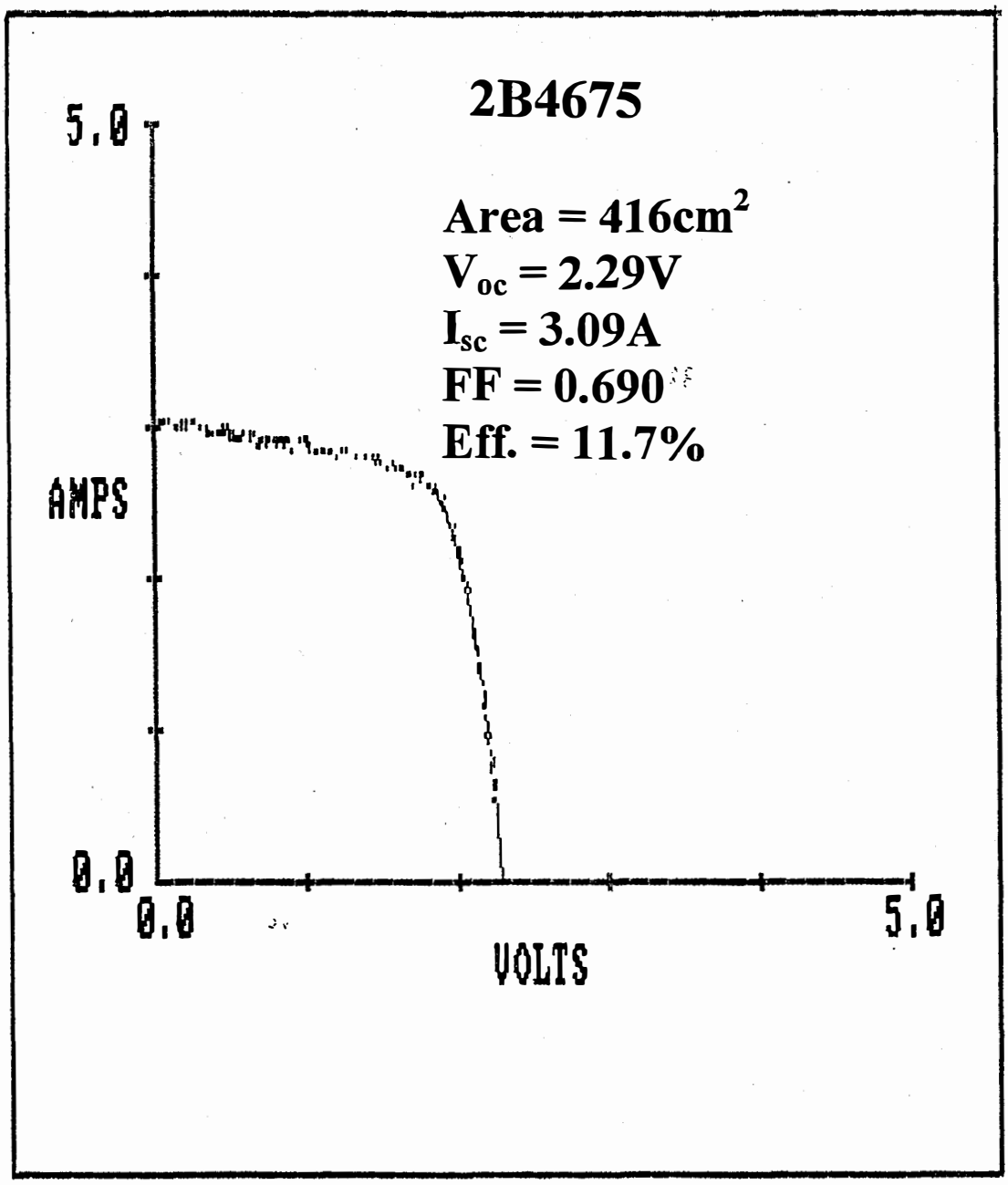

Fig. 10. IV characteristics of 11.7% initial efficiency module.

Section 5

Laser-Processed Module Status

Introduction

In order to reduce the cost of module manufacturing, we need to increase the degree of automation, decrease the cost of module finishing materials, and increase module efficiency. First, a cost reduction in module manufacturing may be accomplished by simply extending the roll-to-roll process as far into the module fabrication line as possible. We may also reduce the cost of module manufacturing by using less expensive materials or reducing the amount of materials utilized. Finally, an increase in efficiency, achieved by a reduction in module parasitic losses, will serve as a cost reducer.

To accomplish these goals, we are developing a laser-interconnected monolithic module process. This laser process has advantages over present fabrication designs in terms of both cost and efficiency. The cost of modules using this laser process will be dramatically reduced because of the high degree of automation obtainable because of the extension of the roll-to-roll process further into the manufacturing line. Also, because of the very small feature heights for this type of module, it will be possible to consider less expensive, more reliable alternative encapsulations that are not possible in the present module designs. The modules produced by this laser process will also have considerably less module losses (shadow, electrical resistance) than present modules, thus making them more efficient. The total module losses can be reduced to near 1% using this approach.

Laser-processed Module

Module Design

In Fig. 11 we show the laser device fabrication process. This module is a parallel laser- interconnected device, unlike other laser-interconnected modules that facilitate series cell interconnections. We begin the process by depositing an insulating layer onto the stainless steel substrate. This layer could be made of many materials, but we have chosen a silicon oxide alloy deposited at high rates in a CVD process. We next deposit the back reflector onto the insulator. We now have a back reflector that is electrically isolated from the stainless steel substrate forming a metal-insulator-metal (MIM) structure. We next drill a matrix of holes, arranged across the surface, through the back reflector and insulator. The back reflector must be cut back further than the insulator such that the diameter of the back reflector hole is larger and approximately concentric with the smaller insulator hole. Therefore, we still have an electrically isolated MIM structure. This is achieved with a single laser pulse. We next deposit the a-Si alloy triple-junction device. This is followed by drilling a second concentric hole through the a-Si alloy device, thereby exposing the stainless steel substrate. The diameter of this hole will be less than the diameter of the back reflector hole to maintain electrical isolation. The next step is to deposit a transparent conducting oxide over the entire surface. The TCO would then make electrical contact to the stainless steel substrate. Finally, we will then be able to encapsulate the surface with a thin-film clear coat, again a CVD deposited silicon oxide alloy or a thin layer of EVA and Tefzel.

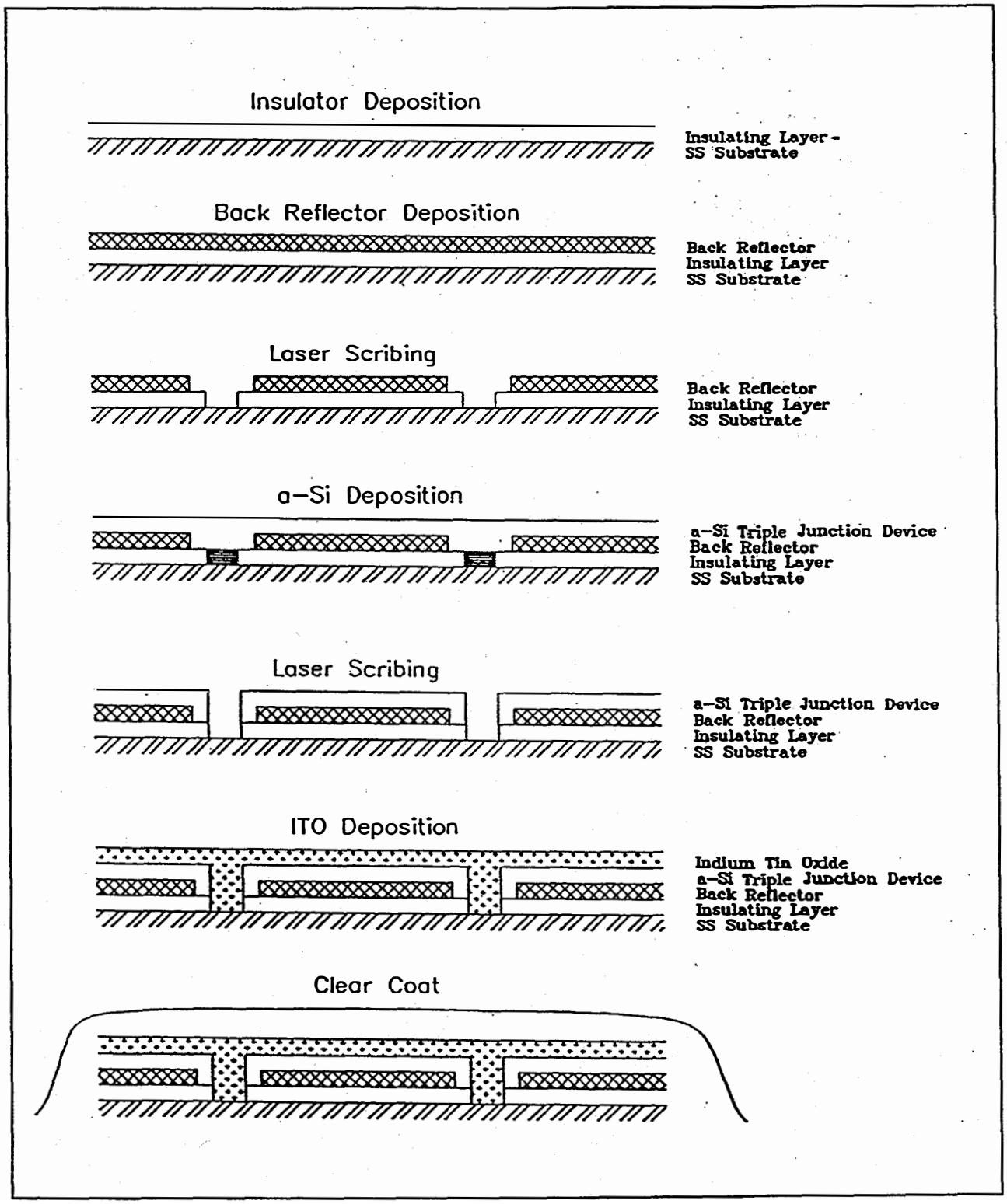

Figure 11. Fabrication process for the laser-interconnected module.

The electrical conduction paths are provided by the TCO and back reflector. The current is collected from the device along the surface by the TCO to the hole and down to the stainless steel now acting as the positive electrode. At the bottom of the device, current is collected from the device and traverses along the back reflector to either edge of the module to the negative electrode. In Fig. 12 we show a multi-plan view of the finished device. It can be seen from the figure that the negative electrode connection takes place on the edge of the module where the back reflector is exposed, either by masking or etching of subsequent depositions.

Given the diameter of the holes at less than 100 μm and hole spacing of 2 mm, we would achieve a shadowing loss of approximately 0.2%. These values, combined with the electrical losses due to transport of current across the TCO and back reflector sheets, give us a total electrical and shadow loss of approximately 1%.

The layout design of the one-square-foot laser-interconnected module is shown in Fig. 13. This drawing shows the laser patterning and thin-film deposition borders as well as contacts. We have fabricated shadow masks for the BR, a-Si, ITO and contact layer depositions to provide access to the BR contacts as well as isolation of the top contact from the BR.

For our prototype module, we start with a piece of .005" thick stainless steel cut to 14" wide by 15.25". We will next punch ¼" registration holes to align the shadow masks in the thin-film deposition processes. The insulator/BR films are then deposited. These films extend out beyond the a-Si alloy device by about 5/8" on two opposite sides in order to trim the tapered edges of the insulator/BR and establish the negative contact to the BR. Contact pads are then deposited on these exposed edges. The pads are segmented to allow for electrical isolation of the back reflector into strips if desired.

The first laser processing occurs after completion of the s.s./insulator/BR and contact pads. This involves cutting continuous lines to segment the BR into sections, if necessary, and drilling through holes into the BR at an appropriate spacing using the laser processor described above. The a-Si alloy device is deposited in-board the BR on the two edges with contacts and flush to the BR on the other two sides. The device is then laser processed by drilling a second set of holes concentric with the BR holes over the entire square foot. The last process is that of depositing the ITO top contact. This layer is deposited completely inside the perimeter of the a-Si alloy device deposition as shown in Fig. 13, completing the thin-film depositions.

The module is then finished by etching a boarder in the ITO layer, if necessary, and passivation of the device. The output interconnects will be made on the contact pads on the two sides of the module. These contacts will be tied together and brought out as output leads. Finally, the module is encapsulated in an EVA/Tefzel lamination.

Laser Processing System

The laser processing system consists of a large-area motion table with sufficient accuracy and speed to process a square-foot laser-interconnected module. This table has 18 inches of x-y travel, 0.5 μm resolution linear encoders, servo motors, precision grade lead screws with anti-backlash nuts, crossed roller ways and an encoder interface for accurate table-to-laser synchronization. On the x-y table, we have mounted precision ground registration pins that will allow us to reproduce substrate position well within .0001". Also mounted on the top axis is a vacuum table hold down to ensure that the substrate, once mounted, is motionless relative to the x-y table. We have specified linear encoders, mounted to each axis, with a pixel resolution of 0.5 μm. These encoders send the encoder interface a digital (5V) pulse every

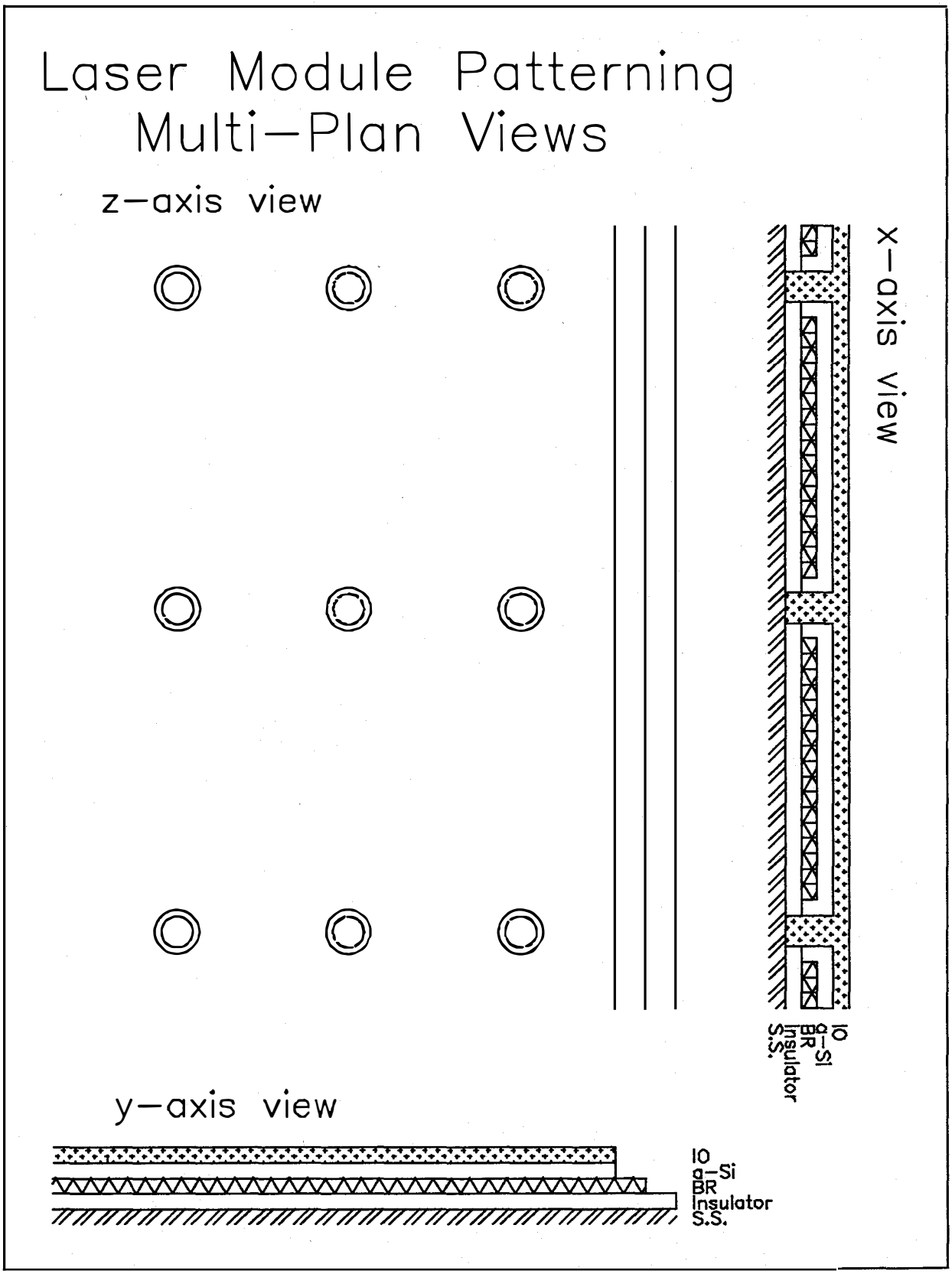

Figure 12. Multi-plan view for the laser-interconnected module.

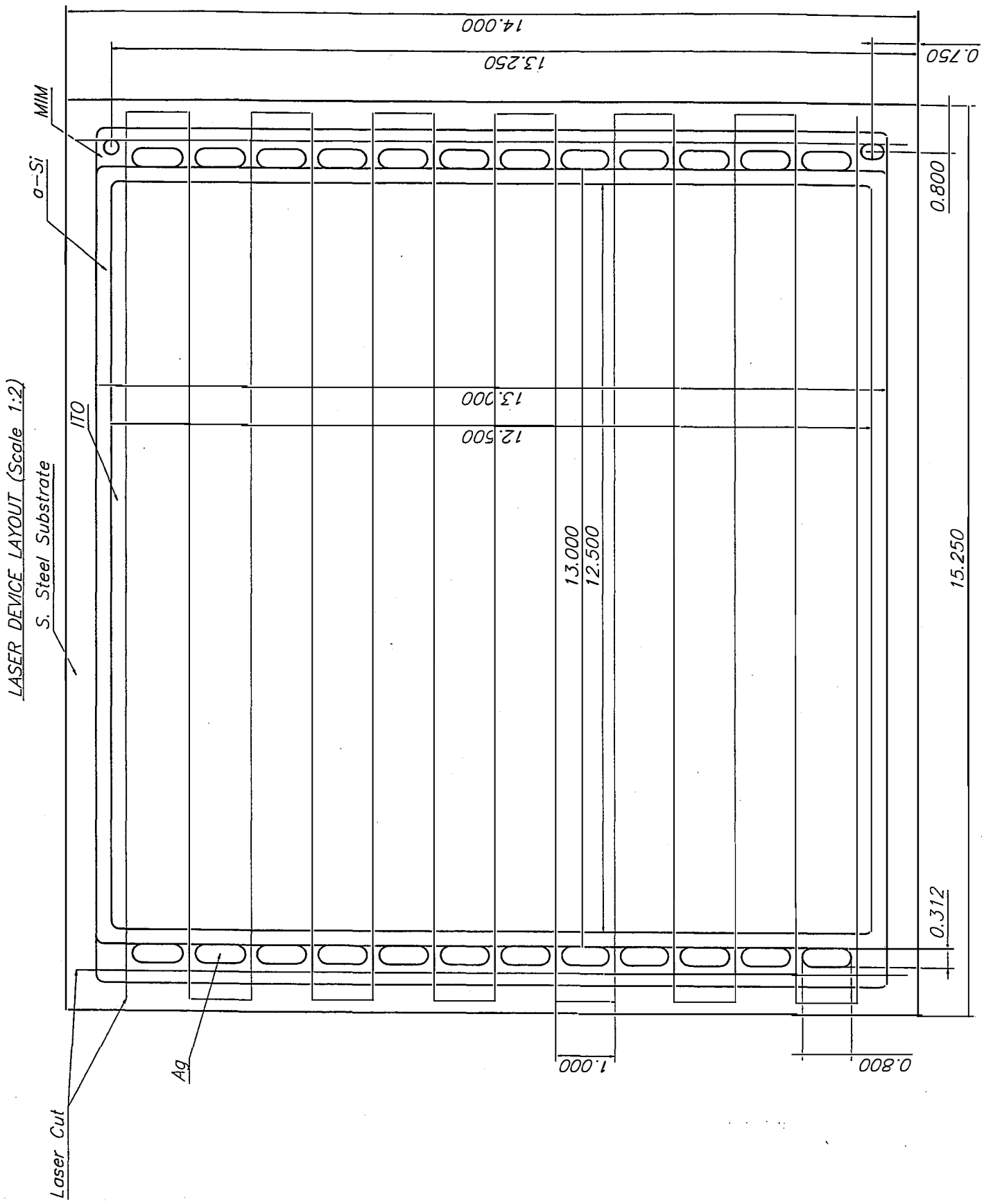

Figure 13. Layout diagram for laser-interconnected module.

Results

Previously we have fabricated a laser-interconnected 12.6 cm^2 triple-junction device measuring 11.5% initial efficiency and 9.8% stabilized efficiency. The device structure was a-Si/a-Si:Ge/a-Si:Ge. The laser fabrication process was similar to the one described in the previous section. We are presently working on scaling this result up to a one-square-foot module. Critical issues in this effort are parasitic losses due to low shunt resistance as a result of debris recast on the BR surface and series resistance due to contact resistances. We have made great strides in the MIM structure in terms of isolation of the two metal contacts. Previously we have struggled to achieve a consistently isolated structure, the results of which were a typically shunted device. We have now fabricated approximately 20 consecutive one-square-foot MIM structures with isolation between metal contacts in excess of 1 $M\Omega\text{-}cm^2$. This has allowed us to more effectively analyze parasitic losses occurring elsewhere in the module structure.

We have now begun to process large-area triple-junction modules using this laser-interconnected process. Several modules of one-square-foot area were successfully fabricated. The series resistance at the point contact was high and thus lowered the efficiency of the module (8.3%). The current of the module was 7% higher than in the conventional modules due to the low shadow losses. This would have the effect of increasing the efficiency of a finished module by approximately a full percentage point. The diameter of the point contacts was approximately 150 μm, with a hole spacing of 2 mm, resulting in an effective shadow loss of under 0.5%. The conventional module has typical shadow loss between 7 and 8%.

Section 6

Reliability Testing

Introduction

We have been testing our modules following IEEE PAR 1262 (Draft 8) which is more stringent than the NREL Interim Qualiication Test (NREL/TR-213-3624). The detailed test sequence is shown in Table 10. Our production modules have passed all the tests. The results have been summarized in the Phase I Annual Report. The 2B modules, which have a similar design, are therefore expected to pass the test, too. Results of "heat cycling," "heat," and thermal cycling tests are reported.

Heat Cycling Test

The "heat cycling" test is essentially an in-house thermal cycling test in which the temperature range for the thermal cycles is approximately 0-90 °C. Two types of modules were fabricated in similar fashion for the test: material obtained from the production machine which uses Al/ZnO back reflector and 2B devices which use Ag/ZnO back reflector. Table 11 summarizes the results of eight modules before and after 180 cycles. The change in efficiency of the three production modules, TA 172, 174, and 176, after the test is within 0.8% of the respective initial values. The corresponding change for the 2B modules, numbers 2B 3972, 3987, 4014, and 4016, is 2.3%. Though the degradation is slightly higher for the 2B samples, it is still within reasonable limits. Module 2B 4036 exhibits an anomalous drop of 8.1% in efficiency.

Heat Test

The "heat" test is an in-house test in which the modules are kept at 90 °C for several hundred hours. The results of the production TA and 2B modules are summarized in Table 12.

The table shows the initial and final values of V_{oc}, J_{sc}, FF, and efficiency and the degradation in efficiency after the test. All the modules survive this severe test. The 2B modules exhibit slightly higher degradation than the TA2 material. Efforts are under way to plug this small difference.

Thermal Cycling Test

This is the conventional thermal cycling test as specified in IQT NREL/TR-213-3624. Two production TA and two 2B modules which had been subjected to 180 "heat cycles" were used for the test. The results after 220 cycles are summarized in Table 13.

The degradation in all cases is within 1.5% of their respective initial values. The modules, therefore, pass the Phase II thermal cycle test milestone. As discussed earlier and as shown in the Phase I Annual Report, the production modules pass all the milestones.

Table 10. PV Module Qualification Test Program.

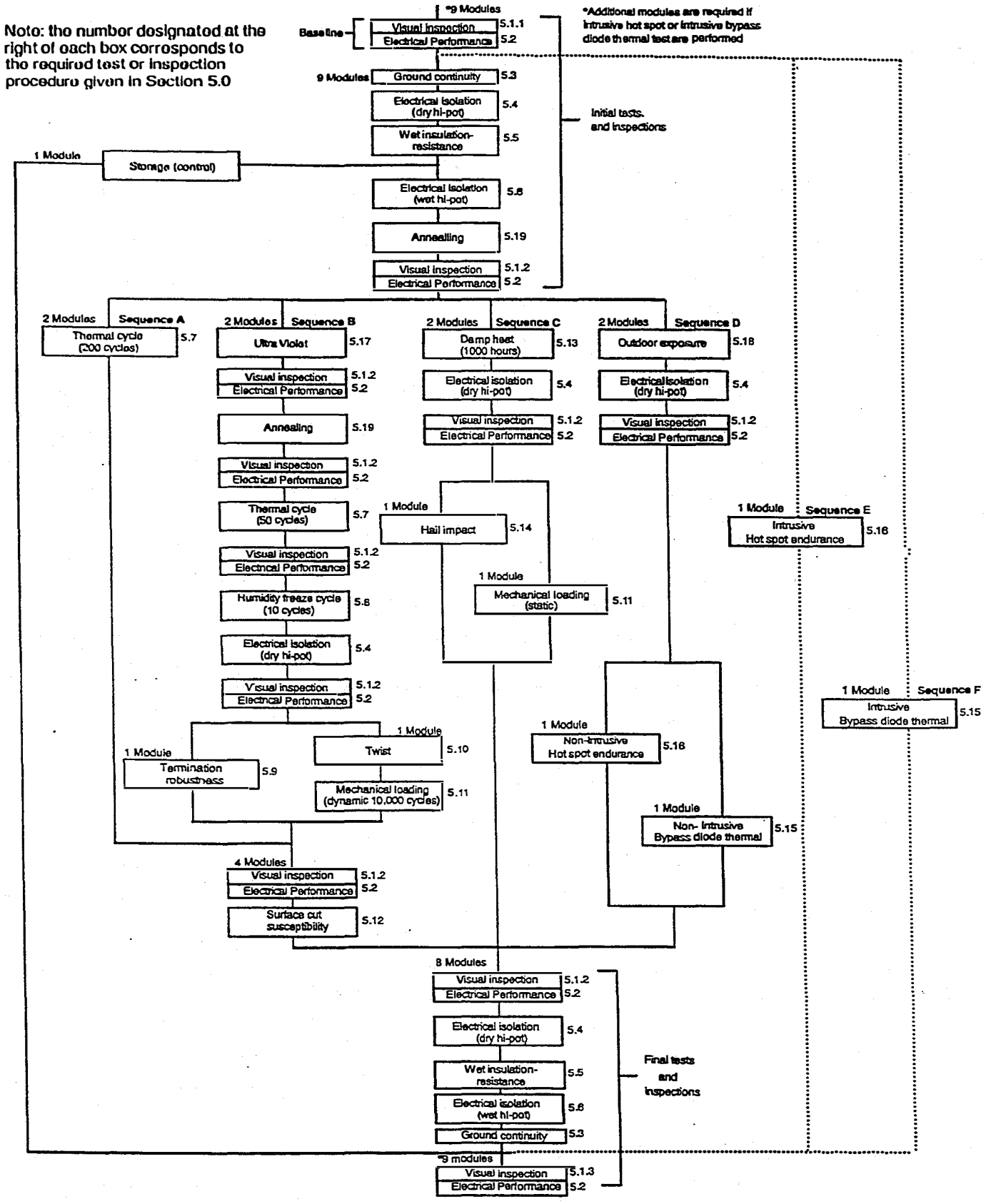

Table 11. Summary of "Heat Cycling" of TA2 and 2B Modules after 180 Cycles.

Module	Status	V_{oc} (V)	I_{sc} (A)	FF	P_{max} (W)	Efficiency (%)	Degradation in P_{max} (%)
TA 172	Initial	1.77	5.67	.652	6.54	7.2	
	Final	1.80	5.60	.652	6.58	7.2	+0.6
TA 174	Initial	1.76	5.62	.658	6.53	7.2	
	Final	1.78	5.56	.654	6.48	7.1	-0.8
TA 176	Initial	1.77	6.14	.651	7.07	7.2	
	Final	1.78	6.13	.642	7.01	7.2	-0.8
2B 3972	Initial	2.34	6.24	.650	9.49	9.7	
	Final	2.34	6.18	.641	9.27	9.5	-2.3
2B 3987	Initial	2.33	6.46	.657	9.88	10.1	
	Final	2.33	6.37	.656	9.73	10.0	-1.5
2B 4014	Initial	2.31	5.92	.655	8.97	9.9	
	Final	2.34	5.86	.651	8.91	9.8	-0.7
2B 4016	Initial	2.32	5.88	.670	9.15	10.1	
	Final	2.34	5.82	.664	9.06	10.0	-1.0
2B 4036	Initial	2.29	5.88	.642	8.64	9.5	
	Final	2.27	5.76	.608	7.94	8.7	-8.1

Table 12. Summary of 90 °C Heat Test of TA2 and 2B Modules.

Module #	Hours	V_{oc} (V)	I_{sc} (A)	FF	Efficiency (%)	Degradation (%)
TA72	0	1.77	5.73	0.661	7.4	
	565	1.80	5.71	0.677	7.5	+1.3
TA67	0	1.76	5.72	0.655	7.3	
	468	1.79	5.61	0.644	7.3	0
TA68	0	1.75	5.60	0.643	6.9	
	468	1.78	5.55	0.654	7.1	+2.9
TA70	0	1.77	5.51	0.670	7.2	
	468	1.81	5.55	0.672	7.4	+2.8
2B4074	0	2.30	5.77	0.666	9.7	
	565	2.32	5.62	0.671	9.6	-1.0
2B4075	0	2.30	5.73	0.655	9.5	
	565	2.32	5.64	0.632	9.1	-4.2
2B4077	0	2.28	5.89	0.654	9.7	
	565	2.31	5.78	0.648	9.5	-2.1

Table 13. Summary of Thermal Cycling of the TA2 and 2B Modules after 220 Cycles.

Module	Status	V_{oc} (V)	I_{sc} (A)	FF	P_{max} (W)	Efficiency (%)	Degradation in P_{max} (%)
TA 172	Initial	1.80	5.60	0.652	6.58	7.2	
	Final	1.78	5.50	0.663	6.50	7.2	-1.2
TA 174	Initial	1.78	5.56	0.654	6.48	7.1	
	Final	1.80	5.56	0.652	6.52	7.2	+0.6
2B 4014	Initial	2.34	5.86	0.651	8.91	9.8	
	Final	2.30	5.79	0.657	8.77	9.6	-1.5
2B 4016	Initial	2.34	5.82	0.664	9.06	10.0	
	Final	2.33	5.78	0.664	8.95	9.8	-1.2

Section 7

Future Directions

We have completed Phase II of the research program and met the major milestones. This has been accomplished by improving the component cell performance over large-area deposition, optimizing the laser-drilling processes and carrying out the relevant reliability studies. The focus of Phase III of the program will be the continuation of the work on large-area deposition. Uniformity issues over large area will be addressed further. Major efforts will be directed toward the development of one-square-foot module using the laser-drilling approach. The main challenge is to reduce series resistance losses at the point contact. Improved deposition methods to obtain good contact between ITO and the stainless steel substrate will be investigated. Further investigations will be carried out on reliability studies, and the aim is to develop the process technology for a low-cost a-Si alloy multijunction module which meets and exceeds the reliability requirement of the users.

Publications

Banerjee, A., Yang, J., and Guha, S. (1997). "Improved Amorphous Silicon Alloy Solar Cells for Module Fabrication." Presented at the Material Research Society Spring Meeting, San Francisco, CA, March 31-April 4.

Glatfelter, T., Lycette, M., Akkashian, E., and Hoffman, K. (1996). "A PV Module with an Active Area Utilization of 99.8%." *Conference Record of the 25th IEEE Photovoltaic Specialists Conference-1996; May 13-17, 1996; Washington, DC.*

Guha, S. (1996). "Amorphous Silicon Alloy Solar Cells and Modules--Opportunities and Challenges." *Conference Record of the 25th IEEE Photovoltaic Specialists Conference-1996; May 13-17, 1996; Washington, DC.*

Guha, S., Yang, J., Banerjee, A., Glatfelter, T., and Sugiyama, S. (1996). "Advances in Amorphous Silicon Alloy Cell and Module Technology." *Proceedings of PVSEC-9; November 11-15, 1996; Miyazaki, Japan.*

Yang, J., Xu, X., Banerjee, A., and Guha, S. (1996). "Progress in Triple-junction Amorphous Silicon Alloy Solar Cells with Improved Current Mismatch in Component Cells." *Conference Record of the 25th IEEE Photovoltaic Specialists Conference-1996; May 13-17, 1996; Washington, DC.*

Yang, J., Banerjee, A., Guha, S. (1996). "A Record Setting Amorphous Silicon Alloy Triple-junction Solar Cell with 14.6% Initial and 12.8% Stable Efficiencies." *Proceedings of the NREL/SNL Photovoltaics Program Review Meeting; November 18-22, 1996; Lakewood, Colorado.*

Yang, J., Banerjee, A., and Guha, S. (1997). "An Amorphous Silicon Alloy Triple-junction Solar Cell with 14.6% Initial and 13.0% Stable Efficiencies." Presented at the Material Research Society Spring Meeting, San Francisco, CA, March 31-April 4.

Yang, J., Banerjee, A., and Guha, S. (1997). "Triple-junction Amorphous Silicon Alloy Solar Cell with 14.6% Initial and 13.0% Stable Conversion Efficiencies." *Appl. Phys. Lett.*, to be published.

REPORT DOCUMENTATION PAGE

Form Approved
OMB NO. 0704-0188

Public reporting burden for this collection of information is estimated to average 1 hour per response, including the time for reviewing instructions, searching existing data sources, gathering and maintaining the data needed, and completing and reviewing the collection of information. Send comments regarding this burden estimate or any other aspect of this collection of information, including suggestions for reducing this burden, to Washington Headquarters Services, Directorate for Information Operations and Reports, 1215 Jefferson Davis Highway, Suite 1204, Arlington, VA 22202-4302, and to the Office of Management and Budget, Paperwork Reduction Project (0704-0188), Washington, DC 20503.

1. AGENCY USE ONLY (Leave blank)	2. REPORT DATE	3. REPORT TYPE AND DATES COVERED
	June 1997	Phase II Annual Technical Progress Report, 2 February 1996 - 1 February 1997

4. TITLE AND SUBTITLE

Thin-Film Amorphous Silicon Alloy Research Partnership; Phase II Annual Technical Progress Report, 2 February 1996 - 1 February 1997

5. FUNDING NUMBERS

C: ZAF-5-14142-01
TA: PV704401

6. AUTHOR(S)

S. Guha

7. PERFORMING ORGANIZATION NAME(S) AND ADDRESS(ES)

United Solar Systems Corporation
1100 West Maple Road
Troy, MI 48084

8. PERFORMING ORGANIZATION REPORT NUMBER

9. SPONSORING/MONITORING AGENCY NAME(S) AND ADDRESS(ES)

National Renewable Energy Laboratory
1617 Cole Blvd.
Golden, CO 80401-3393

10. SPONSORING/MONITORING AGENCY REPORT NUMBER

SR-520-23172

DE97050818

11. SUPPLEMENTARY NOTES

NREL Technical Monitor: K. Zweibel

12a. DISTRIBUTION/AVAILABILITY STATEMENT

12b. DISTRIBUTION CODE

UC-1263

13. ABSTRACT *(Maximum 200 words)*

This report describes the research performed during Phase II of a three-phase, 3-year program. The research program is intended to expand, enhance, and accelerate knowledge and capabilities for developing high-performance, two-terminal multijunction amorphous silicon (a-Si) alloy modules. We discuss investigations on back reflectors to improve cell performance, and investigate uniformity in performance over a 1-sq.-ft. area. We present results on component cell performance, both in the initial and in the light-degraded states, deposited over a 1-sq.-ft. area. The uniformity in deposition is investigated by studying the performance of subcells deposited over the entire area. We also present results on the performance of triple-junction cells and modules. The modules use grid-lines and encapsulants compatible with our production technology. We discuss the novel laser-processing technique that has been developed at United Solar to improve energy-conversion efficiency and reduce manufacturing costs. We discuss in detail the optimization of the processing steps, and the performance of a laser-processed, triple-junction device of 12.6 cm^2 area is presented. We also present experimental results on investigations of module reliability.

14. TERMS

photovoltaics ; thin-films ; amorphous silicon ; triple-junction cells ; laser drilling

15. NUMBER OF PAGES
47

16. PRICE CODE

17. SECURITY CLASSIFICATION OF REPORT	18. SECURITY CLASSIFICATION OF THIS PAGE	19. SECURITY CLASSIFICATION OF ABSTRACT	20. LIMITATION OF ABSTRACT
Unclassified	Unclassified	Unclassified	UL